A NOVEL DIAMOND MICRO PROBE FOR NEURO-CHEMICAL AND -ELECTRICAL RECORDING IN NEURAL PROSTHESIS

Ho-Yin Chan[1], Dean M. Aslam[1], James Wiler[2] and Brendan Casey[2]

[1]Michigan State University, East Lansing, Michigan, USA

[2]University of Michigan, Ann Arbor, Michigan, USA

ABSTRACT

This paper describes the design, microfabrication and testing of a novel polycrystalline diamond (poly-C) based microprobe for possible applications in neural prosthesis. The probe utilizes undoped poly-C with a resistivity in the range of 10^5 Ωcm as a supporting material, which has a young's modulus in the range of 400 – 1,000 GPa and is biocompatible. Boron doped poly-C with a resistivity in the range of 10^{-3} Ωcm is used as an electrode material, which provides a chemically stable surface for both chemical and electrical detections in neural studies. The probe has eight poly-C electrode sites with diameters ranging from 2 to 150 μm; the electrode capacitance is approximately 87 μF/cm^2. The measured water potential window of the poly-C electrode spans across negative and positive electrode potentials and typical has a total value of 2.2 V in 1M KCl. The smallest detectable concentration of norepinephrine (a neurotransmitter) was on the order of 10 nM. The poly-C probe has also been successfully implanted in the auditory cortex area of guinea pig brain for *in vivo* neural studies. The recorded signal amplitude was 30-40 μV and had a duration of 1ms.

1. INTRODUCTION

One of the key components in neural prosthetic systems is the microelectrode/microprobe, which interfaces with neurons for electrical and chemical signal recording, and for stimulation. In early *in vivo* studies, metal wires coated with insulating materials [1] were used as electrodes, which are associated with limited spatial resolution. In the late 1960s, electrodes with multiple recording or stimulating sites were fabricated on microprobes with high reproducibility utilizing lithographic thin-film techniques [1]. With the development of Micro-Electro-Mechanical Systems (MEMS) technologies, sophisticated microprobes with electrode arrays have been developed and are widely used in neural activity studies [2],[3],[4],[5], drug delivery [6],[7], and cochlear implants [8],[9]. Microprobe arrays have been fabricated, microassembled and integrated with a hybrid application specific integrated circuit (ASIC) chip to build a 3D microelectrode array [10]. Nevertheless, most of

them are made out of silicon due to the fact that silicon based bulk micromachining technology is well developed. The silicon microprobes are either fabricated on bulk silicon or silicon on insulator (SOI) wafers. In the former case, highly boron doped silicon is used as the etch stop in the ethylenediamene pyrocatecol (EDP) or Tetramethylammonium hydroxide (TMAH) etching to release the probe structure. On the contrary, the oxide layer of the silicon on insulator (SOI) wafers is used as the etch stop in deep reactive ion etching (DRIE) for probe releasing. Due to the biocompatibility and flexibility issues associated with Si probes, recently, researchers have been studying the use of other materials in the probe fabrication. For example, parylene C [11],[12],[13], polyimide [14] and SU-8 [15] are often used as materials for probe substrate or coating.

The most important component on the microprobes is the metal site, which is used for signal recording and electrical stimulation. Commonly used site materials include platinum [16], gold [17], titanium nitride [18] and iridium oxide [19]. The sites should be inert and chemically stable in the working environment-especially in ion- and protein- rich conditions. Otherwise, the corresponding background noise would be too high, or the target signal could be suppressed due to site blocking caused by residues formed or absorbed on the site surface. For stimulation, the electrode should have a large charge storage capacity as well as charge delivery capacity in order to deliver a large amount of charge in a small geometric area. Sites for recording, on the other hand, should be associated with relatively low background noise in order to achieve a high signal to noise ratio. The exposed site area should be large for collecting more signals in the case of electrical recording. Also, the thermal noise is reduced because of the low impedance of larger sites [20], but the selectivity (i.e. the ability to discriminate signals from different neurons) would be low. Thus, the signal would be from multiple units but not from isolated unit. On the contrary, in electrochemical recording, the site area as well as double layer capacitance has to be small in order to minimzie non-Faradic current which is mostly caused by the charging of the double layer structure formed at the electrode/electrolyte interface. Therefore, in order to have good signal to noise ratio (>3), the electrode should have low capacitance and also wide water potential window (potential range in which there is no current caused by oxygen or hydrogen evolution). Carbon fiber [21] is one of the promising materials for electrochemical detection as it has most of the characteristics mentioned above. However, one of the main disadvantages of carbon fiber is the fouling which requires constant surface polish over a period of time.

In this study, polycrystalline diamond (poly-C) is chosen as the core material in the microprobe due to its unique combination of properties. The presence of unique sp^3 C-C bonds in the diamond lattice leads to its unique mechanical properties (large Young's modulus, $\sim 10^{11}$ Pa). Poly-C has a large band gap (5.5 eV) which makes it a good insulating and optically transparent material [22]. The optical transparency of the diamond substrate is important for *in vitro* experiment because it allows the electrode positions on the probe to be easily located under microscope. In addition, the comparatively

wide total potential window (the reported values range from 1.4 to 4 V) in an aqueous environment [23],[24],[25],[26], low double layer capacitance (ranging from 5 to 40 μF/cm^2) [27], chemical inertness and stability, resistance to fouling of boron-doped diamond make it an excellent site material for microprobes [23]. The biocompatibility of diamond surfaces has been studied intensively based on the protein adsorption and cellular responses on chemical-vapor-deposited (CVD) diamond [28] and diamond-liked carbon (DLC) [29]. It is found that CVD diamond absorbed and denatured relatively small amounts of fibrinogen which is commonly used as a biocompatibility indicator, and there is no cytotoxicity, inflammatory reaction and adverse effects on cells [30]. In electrochemistry, researchers have extensively studied boron-doped diamond as an electrode material [31],[32]. The boron doped poly-C electrodes, used in neural studies [33],[34], were fabricated by depositing diamond on the tip of a wire. These electrodes display limited spatial resolution for studying brain activities. Recently, poly-C sensors and electrodes were integrated in Si cochlear microprobes for the first time [9].

In this paper, diamond based neural probes (poly-C neural probes) are designed, fabricated and tested for the first time. The poly-C neural probes, each having a precisely positioned array of electrodes with micrometer or nanometer dimensions, make it possible to detect multiple chemical and electrical signals with a single probe structure. A unique feature of such probes is that they use undoped poly-C as a mechanical material and boron-doped poly-C as a site/lead material, making it possible to fabricate all-diamond probes.

2. DIAMOND MICROMACHINING TECHNOLOGIES

Important processes in the micromachining of poly-C include diamond seeding, diamond growth and doping, and diamond dry-etching. While the first two processes have been investigated extensively in past studies [35], the optimization of dry etching of diamond has been accomplished for neural probe fabrication for the first time in the current study.

A. Diamond Seeding

The growth of poly-C on non-diamond substrates such as Si requires a pretreatment step to generate seeds (or nuclei) on the substrate [36]. In this study, diamond-loaded water (DW) is used to nucleate the Si surface. The powder size is 0.1 μm on average. The seeding density (and grain size after poly-C growth) are related to the spin rate and diamond particle density in the DW [37]. The DW was applied to the substrate with a 500 rpm pre-spin for 10 sec followed by 2000 rpm for 30 sec. This process ensures a uniform seeding density over the entire 4" wafer. As the first step in the poly-C neural probe process, depending upon the type of probe, is poly-C growth either directly on Si or oxidized Si surface, silicon's hydrophobic surface makes it difficult to have a uniform seeding density on bare Si surface as shown in Fig. 1(a). A thin layer of SiO_2 grown or

deposited on Si can solve this problem. It has been reported [38] that the first half of RCA-clean (NH_3:H_2O:H_2O_2, HCL:H_2O:H_2O_2) chemically oxidizes the Si surface, which makes it hydrophilic. Thus, prior to the application of DW, the cleaning of Si surface through first half of the RCA cleaning process improves the uniformity of DW seeding as shown in Fig. 1(b). The resulting seeding density is in the range of 10^9 – 10^{10} cm^{-2}. If the fabrication process starts on an oxidized Si surface the uniformity of DW is not a problem.

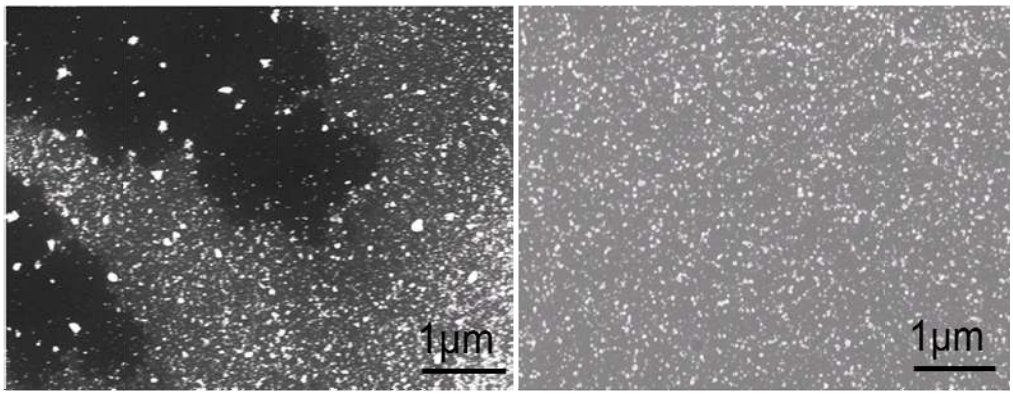

(a) **(b)**

Fig. 1. Seed distribution on (a) a non-treated and (b) an RCA-treated Si surface.

B. Diamond Growth and Doping

Microwave Plasma Chemical Vapor Deposition (MPCVD) was used for the poly-C growth using parameters shown in TABLE I [37]. The diamond film was in-situ boron doped by introducing trimethylboron (TMB), ($B(CH_3)_3$), gas diluted in hydrogen. The boron doping level, according to data presented in [37], is in the range of 3000 - 7000 ppm (B/C ratio in gas phase); the resistivity is in the range of 10^{-1} - 10^{-3} Ωcm. The average grain size on the surface of the poly-C film is approximately 2 μm. The film quality, as indicated by the sp^3/sp^2 C-C bond ratio, is very good as indicated by the sharp Raman peak shown in Fig. 2.

As poly-C is grown at 750°C, hydrogen plasma continues to etch SiO_2 through the holes between the diamond seeds until it is fully covered by poly-C. This can cause problems if the SiO_2 layer is used as an insulating layer. The etch rate of different types of commonly used SiO_2 layers are listed in TABLE II. A knowledge of time required to form a continuous film, t_c, is important if SiO_2 is used as an insulator. This time, t_c, is plotted as a function of spin speed for DW as shown in Fig. 3. The resulting seeding density is also plotted. It is noted that as the spin speed increases, the seeding density decreases which leads an increase in t_c.

TABLE I

Conditions for Diamond Growth Using MPCVD

Parameter(s)	**Value(s)**
Growth Temperature	750 ^{o}C
Growth Pressure	40 Torr
Gases Used for Growth	Methane: 1 sccm Hydrogen: 100 sccm
Dopant Used for B-doped Poly-C	Trimethylboron diluted in H_2 (0.1% of $B(CH_3)_3$ by volume in H_2): 5-10 sccm
Microwave Power Used for Growth	2.3 kW, 2.4 GHz
Growth Rate	0.10 - 0.15 µm/h
Poly-C Film Thickness; Undoped/Doped	3 µm/ 0.5 µm

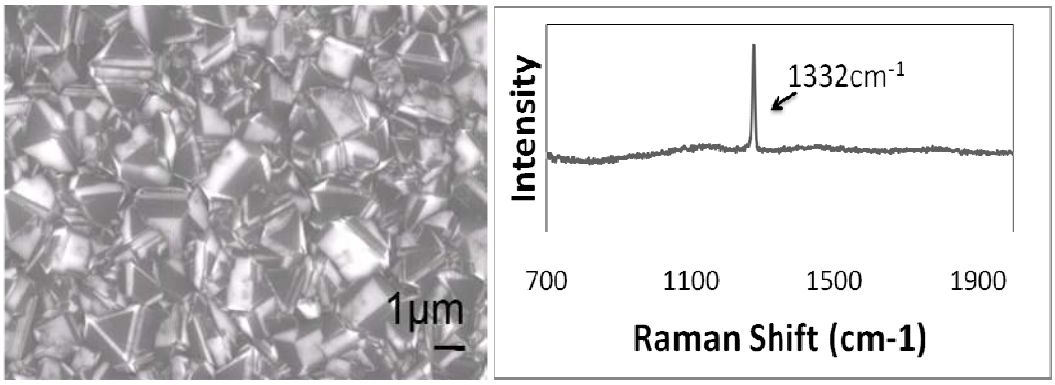

(a) (b)

Fig. 2. (a) An SEM image of a poly-C surface and (b) its Raman spectrum.

TABLE II

Etch rates of un-annealed SiO_2 during poly-C growth.

SiO_2 Growth/Deposition		**SiO_2 Etch Rate (nm/min) at Poly-C Growth Temperature of 750 ^{o}C**
Method	**Temperature (^{o}C)**	
Thermal	1100	1.0 - 3.0
LPCVD	450	1.4 - 3.1
PECVD	380	2.8 - 4.4

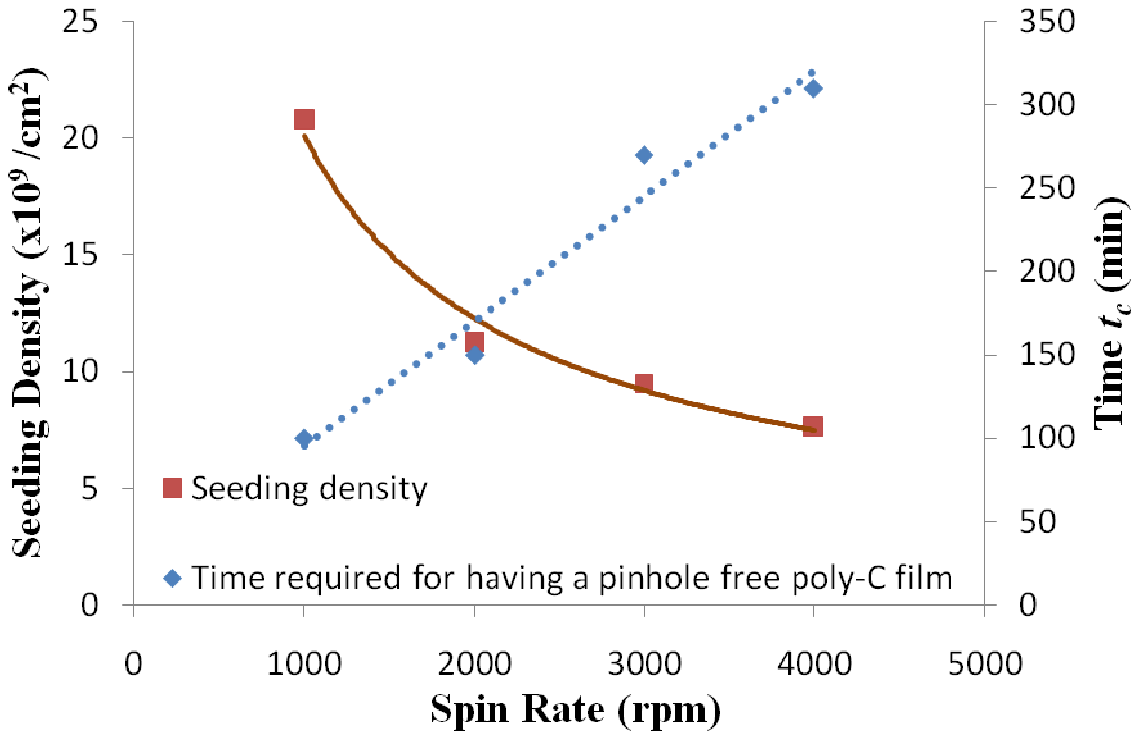

Fig. 3. The relationships between the seeding density and time t_c as a function of seeding spin rate.

C. Diamond Dry Etching

Although the reactive ion etching of diamond has been studied intensively [39],[40],[41], poly-C dry etching used in the neural probe fabrication in the current work (see TABLE III) has been problematic. SEM micrographs taken at different stages of dry etching of poly-C are shown in Fig. 4. As the etching of poly-C continues to reach the seeding portion of the poly-C film, holes appear in the poly-C film as seen in Fig. 4(c). At this stage of etching process, if the etching gases contain fluorine, the underlying substrate (Si or SiO_2) is etched which increases its roughness. However, in the absence of fluorine, it is well known that micro columns (due to micromasking) would be formed in the etching gases [42], which is due to sputtering of Al by O_2 plasma. The showering of sputtered Al particles on the surface being etched leads to micromasking. A two step etching process was developed to eliminate micromasking and substrate etching [43]. First, poly-C is etched in the presence of only CF_4 until a very thin poly-C film is left on the surface. Then, the final etching stage is done in pure oxygen. This process leads to smooth Si or SiO_2 surface with a roughness of approximately 3 nm.

TABLE III

Parameters for Diamond Etch

Parameter(s)	**Value(s)**
Power	300 W
Pressure	50 Torr
Gases	O_2: 40 sccm Tetrafluoromethane (CF_4): 1 sccm
Bias	293V
Etch rate	1.2 µm/h

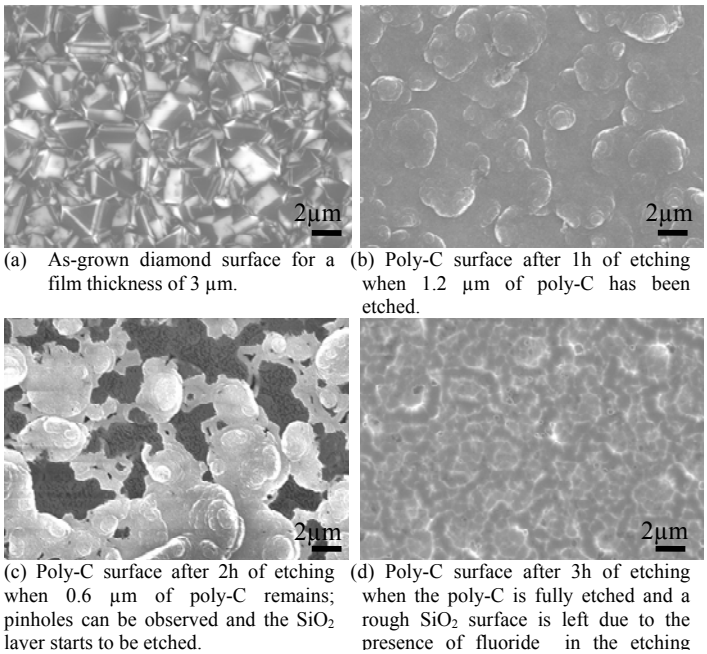

(a) As-grown diamond surface for a film thickness of 3 µm.

(b) Poly-C surface after 1h of etching when 1.2 µm of poly-C has been etched.

(c) Poly-C surface after 2h of etching when 0.6 µm of poly-C remains; pinholes can be observed and the SiO_2 layer starts to be etched.

(d) Poly-C surface after 3h of etching when the poly-C is fully etched and a rough SiO_2 surface is left due to the presence of fluoride in the etching

Fig. 4. SEM images of the diamond surface at different stages of the etching process.

3. DESIGN AND FABRICATION OF DIAMOND PROBES

A schematic of the probe depicted in Fig. 5(a) reveals details of the probe dimensions used in the design, which requires a six-mask fabrication process. The fabricated probe shank is translucent and flexible as shown in Fig. 5(b) and (c). Several designs of the diamond probe have been studied ranging from all-diamond (the shank is made out of poly-C only) to diamond. The probe shown in Fig. 5(a) has eight highly boron doped poly-C sites with diameters ranging from 2 to 150 µm [44].

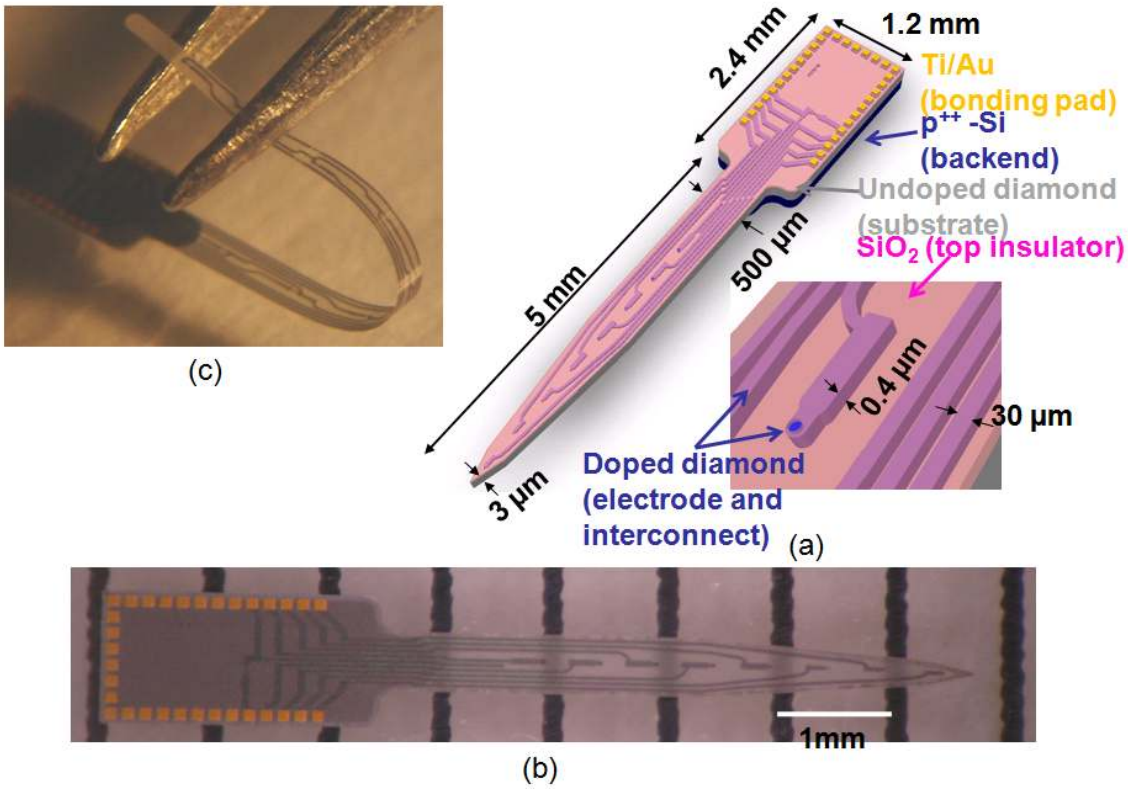

Fig. 5. (a) Schematics of the diamond probe, (b) fabricated probe, and (c) probe bent through 180 degrees.

Shown in Fig. 6 are the general process flows of two types of probes - the all-diamond and diamond probes. The probes are referred to as all-diamond if the shank is made out of poly-C only meaning that sites, leads and probe substrate are all made from poly-C. Some all-diamond probes do not use p^{++}-Si as a support material at their backend. It is important to point out that all probe structures, referred to as all-diamond probe or diamond probe, studied in this work use undoped poly-C as a structural material (in shank and backend), Ti/Au as contact pad material (at the backend) and p^{++}-Si as a support material at their backend. Since the all-diamond probe is a new concept, its efficacy as a neural probe is investigated using different lead, site and insulating materials. The resistivity of poly-C, used as site and lead material, is in the range of $5 \times 10^{-2} – 10^{-3}$ Ω·cm

[37],[44]. The undoped poly-C resistivity is in the range of 10^5 – 10^8 Ωcm [44]. Normally, all-diamond probes can only be used for electrical detection and stimulation applications. For chemical detection the frontend has a reference electrode that is made of Ag/AgCl. The probes are termed as diamond probes if the frontend has sites, leads and/or insulating layers that are not made from poly-C, but the later is still used as a structural material.

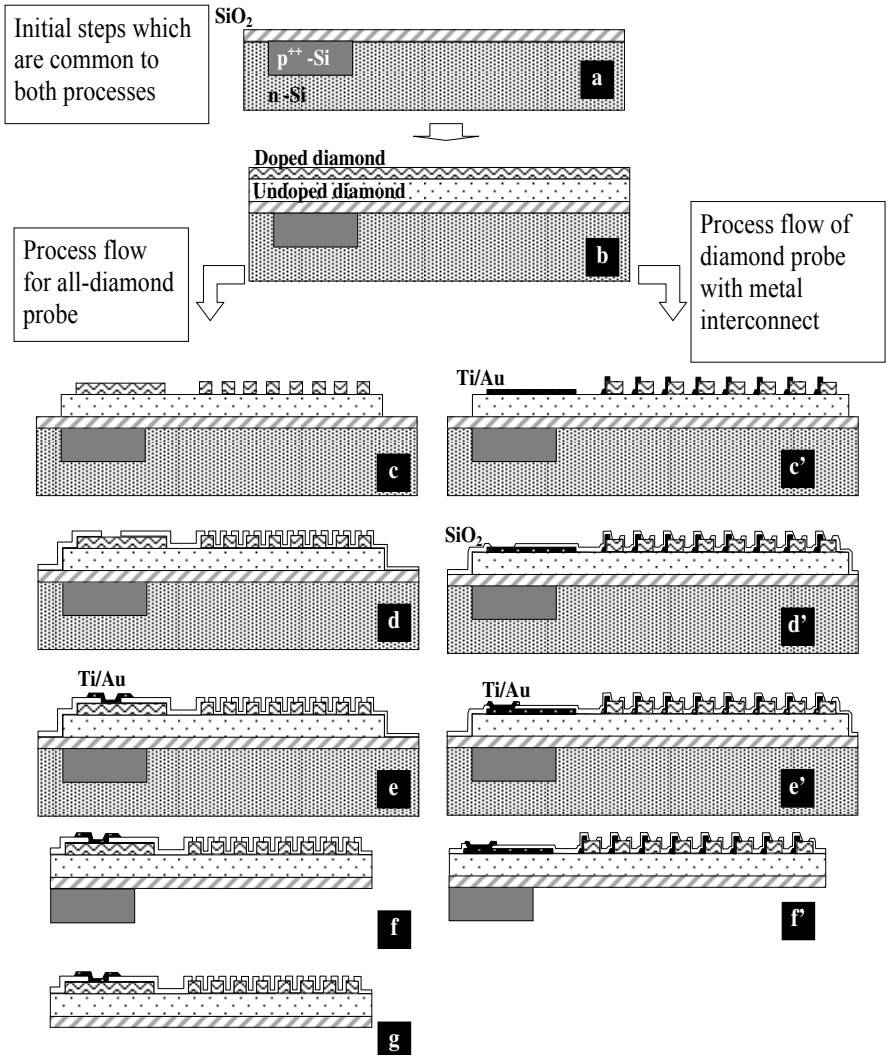

Fig. 6. Fabrication processes of all-diamond and diamond probes; (a) creation of 10 µm thick highly boron-doped silicon region followed by growth of 2 µm thermal oxide, (b) growth of 3 µm undoped and 0.5 µm doped poly-C, (c) poly-C patterning using RIE, (d) 1µm PECVD oxide deposition and patterning for top insulation, (e) patterning of 300 x 300 μm^2 Ti/Au contact pads, (f) probe released by EDP etching, and (g) removal of p^{++}-Si layer

As the growth of undoped poly-C directly on boron-doped Si leads to boron out-diffusion from Si and incorporation in poly-C increasing its conductivity, a layer of SiO_2 was used to seal the boron out-diffusion. It is found that the difference in

the resistivities of diamond films on Si substrate with and without SiO_2 protection can be 2 orders in magnitude. Therefore, SiO_2 is an essential layer for diamond growth on a boron doped silicon substrate (Fig. 6(a)). A 1.5 μm thick thermal oxide is needed to suppress the boron out-diffusion by taking into account the fact that SiO_2 can be etched during the initial phase of poly-C growth when the poly-C film is not continuous. Aluminum (700 nm) was used as the mask for dry etching (Fig. 6(c)). The etching of the undoped/highly doped diamond stack was monitored by measuring the resistivity of the etched surface and the step height of the patterns. As the resistivity exceeds 10^5 Ωcm, the doped poly-C has been fully etched. The undoped poly-C serves as the substrate for the probe, while the highly doped poly-C is for the sites and leads. In the case of using metals as the lead material, an additional step is added to pattern a Ti/Au (50nm/300nm) layer (Fig. 6(c')). Then, a 1.4 μm PECVD SiO_2 layer was deposited. This layer was patterned and etched using a buffered oxide solution in order to expose the contact pads (located on the backend) and the diamond sites (Fig. 6(d) & (d')). A layer of titanium/gold (50 nm/300 nm) was then deposited and patterned to form the contact pads (Fig. 6(e) & (e')). Finally, the Si substrate was thinned by HF-nitric (HNA) down to 200 μm and the probes were released using the ethylene-diamine-pyrocatechol (EDP) process (Fig. 6(f) & (f')) with boron etch stop. For some probes the p^{++}-Si layer was removed (Fig. 6(g)).

4. EXPERIMENTAL RESULTS AND DISCUSSIONS

The testing of poly-C neural probes consisted of electrode modeling, electrode comparison, chemical detection and *in vivo* electrical detection. A potentiostat (model # CH750C by CH Instruments) with a three electrode configuration (working, counter and reference electrodes) was used for electrochemical measurements and a Faraday cage was used for minimizing the surrounding noise. Electrical Impedance Spectroscopy (EIS) was used for electrode modeling and characterizing the electrode behavior in a wide range of frequencies [45],[46]. Cyclic Voltammograms (CV) were used for studying the electrode reactions, which give information not only on the thermodynamics at reactions but also on kinetic parameters (e.g. heterogeneous electron-transfer rate constant). The working, counter and reference electrodes were diamond, platinum and Ag/AgCl, respectively. The potential sweep rate is 100 mV/s.

The *in vivo* electrical detection was done in the Kresge Hearing Research Institute at the University of Michigan and performed on pigmented guinea pigs using approved animal use and care procedures. The poly-C probe was placed in the auditory cortex in the right hemisphere of the guinea pig's brain, which was connected to a Plexon Neural Data Acquisition System to record the stimulated neural signals.

A. Poly-C Electrodes/Electrolyte Interface

It is well known that an electrical double layer is formed by electrons in the metal and ions close to its surface when an electrode is placed in an electrolyte. This interface acts like a capacitor which charges or discharges depending on the imposed voltage. It also affects the electrode's ability to deliver charge (in electrical stimulation) and its background current (in electrical and electrochemical detection). Based on the circuit model shown in Fig. 7 with constant phase elements replacing the Warburg impedance W and double layer capacitance Q, the total impedance is given by,

$$Z = R_s + \frac{Q(R_t+W)}{W+Q+R_t} \tag{1}$$

where $Q = \frac{1}{(j\omega C_{dl})^{\alpha}}$, $W = \frac{1}{(j\omega C_w)^{\beta}}$ and $0 \le \alpha, \beta \le 1$.

The real and imaginary parts of the total impedance are given by (2),

$$\boldsymbol{Z} = \underbrace{\left(\boldsymbol{R_s} + \frac{\boldsymbol{B^2R_t+ABR_t\sin\left(\frac{(\alpha+\beta)\pi}{2}\right)+Bsin\left(\frac{(2\alpha+\beta)\pi}{2}\right)+Asin\left(\frac{(\alpha+2\beta)\pi}{2}\right)+R_t\cos\left(\frac{(\alpha+\beta)\pi}{2}\right)+BR_t^2\cos\left(\frac{\alpha\pi}{2}\right)}}{\boldsymbol{B^2+A^2+R_t^2+2AB\sin\left(\frac{\alpha+\beta}{2\pi}\right)+2BR_t\cos\left(\frac{\alpha\pi}{2}\right)+2AR_t\cos\left(\frac{\beta\pi}{2}\right)}}\right)}_{\boldsymbol{Z'}} + \boldsymbol{j}\underbrace{\frac{\boldsymbol{ABR_t\sin\left(\frac{(\beta-\alpha)\pi}{2}\right)-Bsin\beta-Asin\alpha-R_t\sin\left(\frac{(\alpha+\beta)\pi}{2}\right)}}{\boldsymbol{B^2+A^2+R_t^2+2AB\sin\left(\frac{\alpha+\beta}{2\pi}\right)+2B_t\cos\left(\frac{\alpha\pi}{2}\right)+2AR_t\cos\left(\frac{\beta\pi}{2}\right)}}}_{\boldsymbol{Z''}} \tag{2}$$

The phase of Z can be computed by $\tan^{-1}(\frac{Z''}{Z'})$ which becomes,

$$\theta = \tan^{-1}\frac{ABR_t\sin\left(\frac{(\beta-\alpha)\pi}{2}\right)-Bsin\beta-Asin\alpha-R_t\sin\left(\frac{(\alpha+\beta)\pi}{2}\right)}{B^2R_t+ABR_t\sin\left(\frac{(\alpha+\beta)\pi}{2}\right)+Bsin\left(\frac{(2\alpha+\beta)\pi}{2}\right)+Asin\left(\frac{(\alpha+2\beta)\pi}{2}\right)+R_t\cos\left(\frac{(\alpha+\beta)\pi}{2}\right)+BR_t^2\cos\left(\frac{\alpha\pi}{2}\right)} \tag{3}$$

where $A = (\omega C_{dl})^{\alpha}$ and $B = (\omega C_w)^{\beta}$.

At low frequencies, the total impedance Z is dominated by the Warburg impedance (due to the mass transfer of ions to and from the electrode) and becomes,

$$\boldsymbol{Z_l = R_s + R_t + \frac{1}{(j\omega C_w)^{\beta}}} \tag{4}$$

This corresponds to a straight line with a slope of $\tan(\frac{\pi\beta}{2})$ in the Nyquist plot.

On the other hand, at high frequencies, the effect of the Warburg impedance is no longer significant as compared to the double layer capacitance. Therefore, the total impedance becomes,

$$\boldsymbol{Z_h = R_s + \frac{R_t}{1+R_t(j\omega C_{dl})^{\alpha}}} \tag{5}$$

This corresponds to the semi-circle in the high frequency range of the Nyquist plot.

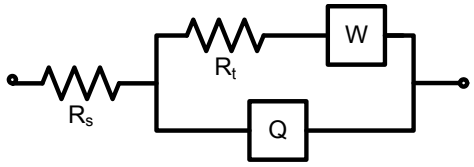

Fig. 7. Electrode/Electrolyte interface model by Randles [45].

To measure the impedance, the poly-C probe was placed in 0.9% saline solution (9000 mg NaCl: 1000 ml DI H_2O); the poly-C electrode acted as the working electrode. The reference and counter electrodes were commercially available Ag/AgCl and platinum electrodes, respectively. A small signal of 5 mV (AC) was applied to the poly-C electrode to record the real and imaginary parts of the total impedance *Z*. The Nyquist and Bode plots in the frequency ω range of 0.1 – 100 kHz are shown in Fig. 8. The predicted total impedance is described by (2). Least squares curve fitting was preformed to obtain the model parameters (R_s, R_t, W and Q). The error is defined as:

$$\boldsymbol{e} = \sum_{i=1}^{N} \frac{\left(Z_{predicted,i} - Z_{measured,i}\right)^2}{Z_{measured,i}^2} \tag{6}$$

where *N* is the total number of data points.

In this method, the function *e* is minimized by adjusting the model parameters; the optimal parameters are listed in TABLE IV. At low frequencies (< 4 kHz), both the real and imaginary parts of the total impedance *Z*, decrease with increasing frequency, and Z has a negative phase θ as shown in Fig. 8(a). This indicates that the electrode behaves capactively. This low frequency behavior is described by the Warburg impedance term, in (4), which is defined as a constant phase element (β=0.43). This describes the ions movement in the bulk solution to and from the electrode interface. The impedance becomes more resistive (i.e. θ changes from -23^o to -15^o) as the frequency increases as shown in Fig. 8(b). The cutoff frequency is around 4 kHz at which point the impedance enters the high frequency regime which can be described by (5); θ reaches its minimum. The impedance becomes more capacitive again (i.e. θ changes from -15^o to -50^o) at high frequencies (> 4 kHz) as shown in Fig. 8(b). In this region, the double layer capacitance *Q* and charge transfer resistance R_t dominate in the total impedance *Z*. In other words, the current is mainly due to the charging of the double layer at the electrode/electrolyte interface at high frequencies. It is noted that there is no further decrease in θ within the measurable frequency range of the equipment. Thus, the poly-C electrode behaves similar to a capacitor within the frequency range of 0.1 – 100 kHz for small signal perturbations. The measured double layer capacitance C_{dl} is ~87 μF/cm^2 which is in the range of reported values (3 - 100 μF/cm^2) [47],[48]. This normalized capacitance is calculated using the geometric area of the electrode. In the case of the poly-C electrode, the effect of its surface roughness on the capacitance can be significant- especially in the high frequency regime. This is because the thickness of the interfacial double layer structure can be less than 5 nm [6]. Thus, the true double layer capacitance can be lower by a factor of 3 to 10 if the roughness of diamond is considered [47]. Polishing the diamond surface is one way to address this issue. Despite its roughness, diamond electrodes are known to have low double layer capacitance as compared to most metal electrodes [49]. This helps keep the RC time constant low. Therefore, the time needed to charge and discharge the double layer structure is small which is essential in *in vivo* electrochemical detection as fast scan voltammetry is often used. Also, the background current, as discussed in the next

section, can be lower due to the small double layer capacitance.

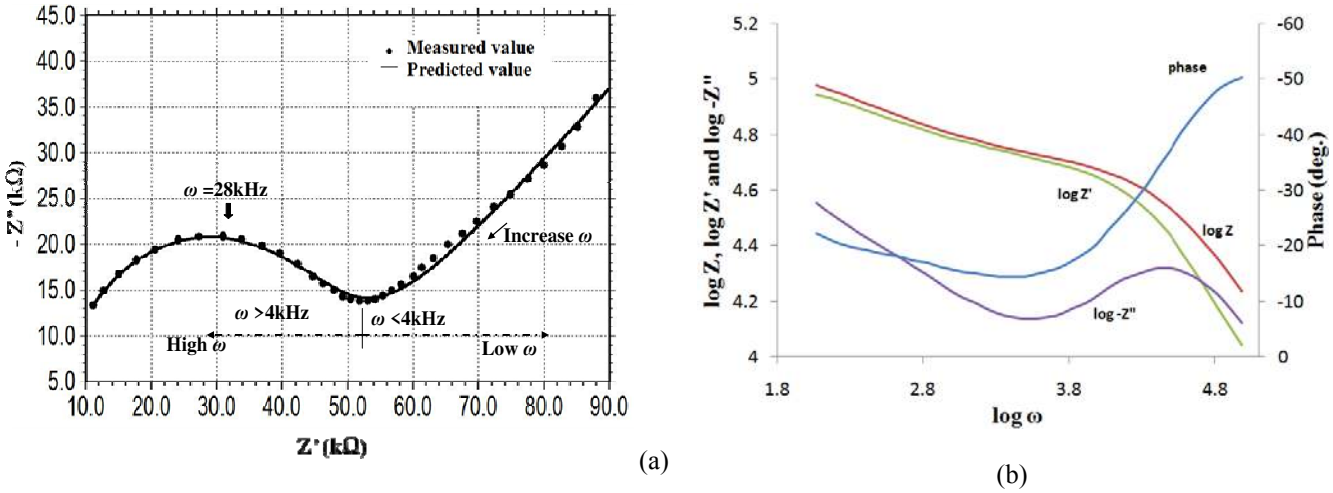

Fig. 8. Impedance spectrum for a diamond electrode with diameter 30 µm, (a) Nyquist plot of the real and imaginary part of the measured impedance, (b) Bode plot.

TABLE IV
Fitted Parameters for Electrode/Electrolyte Model

Parameters	**Values**
Spreading resistance R_s (Ω)	4953(=0.03 Ωcm^2)
Charge transfer resistance R_t(Ω)	4.02x10^4 (=0.284 Ωcm^2)
Warburg impedance W (S sec$^{\beta}$)	2.22x10^{-6} (β=0.43)
Constant phase impedance Q (S sec$^{\alpha}$)	1.12x10^{-9} (α=0.95)
Double layer capacitance C_{dl} (µF/cm^2)	87.45

B. Electrochemical Characterizations of Poly-C Electrodes

In order to compare the performance of diamond electrodes with other electrodes commonly used in neural studies such as Au, Pt and IrO_x electrodes, a 300 nm thick film of Au, Pt or Ir was deposited on highly doped Si samples for CV measurement. The exposed electrode area was 0.2 cm^2. IrO_x was formed by activating Ir in phosphate buffered saline (PBS) solution [50]. The background current of the electrodes in potassium chloride (KCl), Krebs and PBS solutions are shown in Fig. 9. It is found that IrO_x has the largest background current in all the solvents and shows several peaks due to reduction-oxidation reactions that involve the transfer of electrons across the interface [51]. As evident from Fig. 9, IrO_x has not only a high charge storage capacity but also a large charge injection ability, making IrO_x as a material of choice for cell stimulation. The reason of the high Q_{in} of IrO_x is that the mechanism of its charge injection is the faradaic reduction and oxidation between the Ir^{3+} and Ir^{4+} states of the oxide, which correspond to the peaks of the CV as shown in Fig. 9, at the electrode

surface [25]. Poly-C, on the other hand, shows no peak and the lowest background current among the materials. This is an advantage-especially for electrochemical detection because its surface is chemically inert and stable.

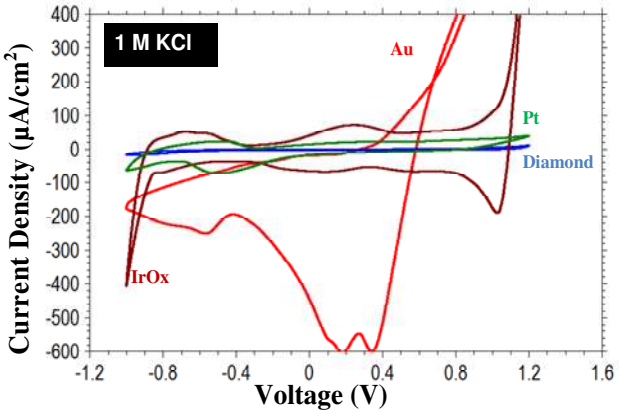

(a)

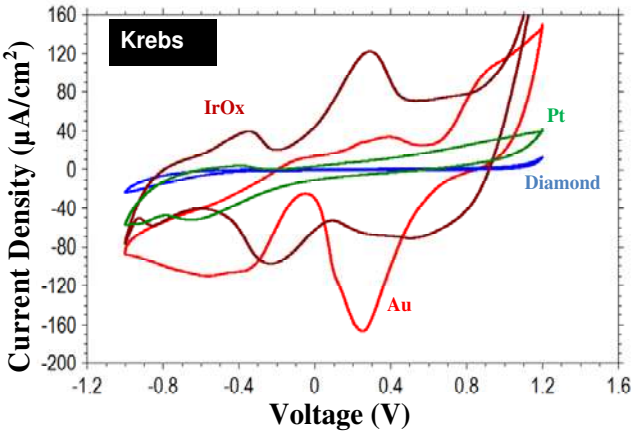

(b)

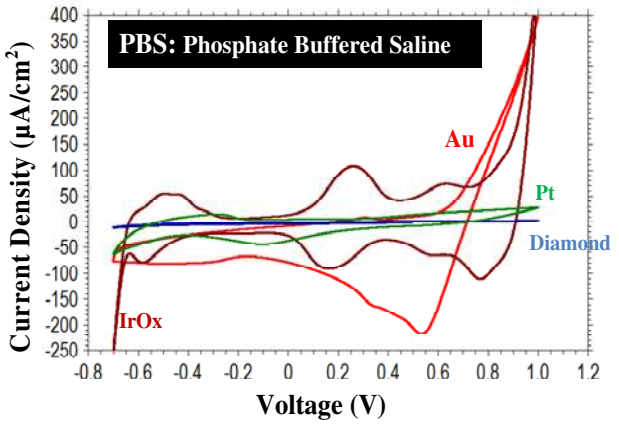

(c)

Fig. 9. Voltammograms of Au, Pt, IrOx and diamond electrodes in (a) 1MKCl, (b) Krebs, and (c) PBS.

In addition to low background current, poly-C electrodes also exhibit a wide water potential window. As shown in Fig. 10(a), the diamond site on the probe reveals a potential window from -0.8 to 1.4 V in 1M KCl, which indicates a high over-

potential for both oxygen and hydrogen evolution. In other words, there is no current caused by oxygen and hydrogen evolution which would interfere with current from target species undergoing redox reaction within this range. As a result, more species can be detected within this potential range.

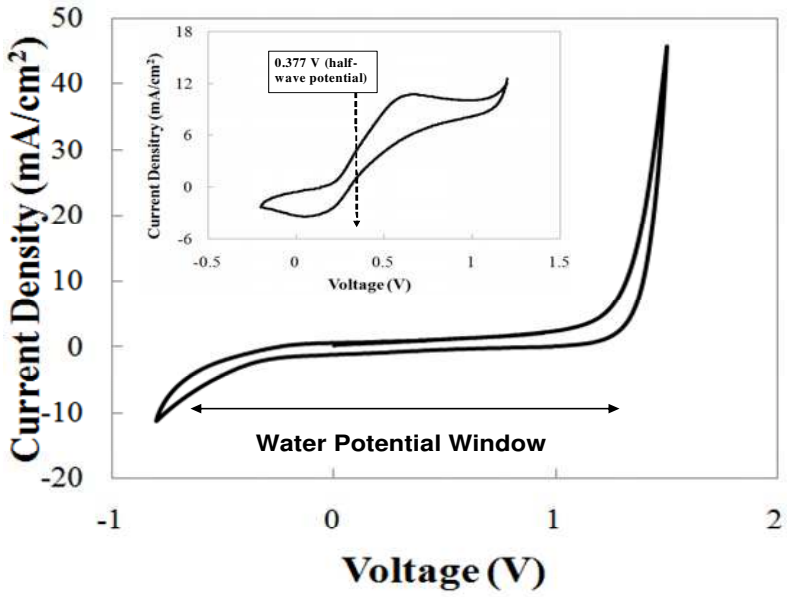

Fig. 10. Cyclic voltammetry current-voltage curve for the diamond probe in 1M KCl. The insert is the CV of the diamond probe in 1 mM $Fe(CN)_6^{-4}$ in 1M KCl. The scan rate was 100 mV/s. The reference and counter electrodes are Ag/AgCl and platinum, respectively**.**

In electrochemistry, the $Fe(CN)_6^{-3/-4}$ redox system has been widely used to evaluate the reactivity of electrodes as they undergo electron transfer via a simple outer-sphere mechanism. In addition, physical and chemical properties of the diamond make the surface highly sensitive to this $Fe(CN)_6^{-3/-4}$ redox system [23]. Thus, this redox system can help determine the quality of diamond electrodes. The corresponding cyclic voltammogram shown in Fig. 10(insert) reveals the half-wave potential $E_{1/2}$ which is indicated by the peak at 377 mV (vs. Ag/AgCl). This figure falls within the range (~ 250 mV to 450 mV) for a typical diamond electrode.

C. Electrochemical Detection Using Diamond Probes

Norepinephrine (NE) is a neurotransmitter which can be found in the sympathetic nervous system and acts as a stress hormone. Norepinephrine, detected electrochemically according to the following $2e^-/2H^-$ redox reaction, is oxidized to form NE-*o*-quinone.:

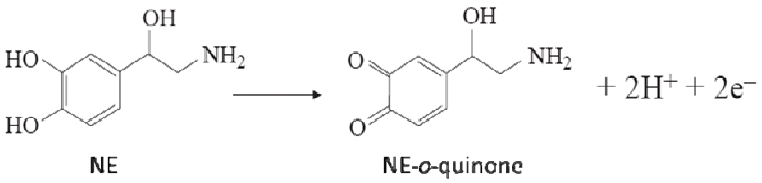

(7)

In a preliminary study focusing on the detection of NE in Krebs buffer solution, current density was recorded as a function of voltage applied to the poly-C electrode with respect to an Ag/AgCl reference electrode. The recorded data shown in Fig. 11 are presented after subtracting the background current (as shown in the inset of Fig. 11) in Krebs solution. The curves shown in Fig. 11 are the currents recorded at different NE concentrations. The recorded current started to increase when the applied voltage reached ~0.2 V. The lowest detectable concentration of NE is roughly 10 nM. The results are similar to those reported in [34] for diamond coated electrodes but there is no peak observed in the recorded current using the poly-C electrode. One possible reason for this could be the variation in diamond quality which leads to a small heterogeneous rate constant k^o [25].

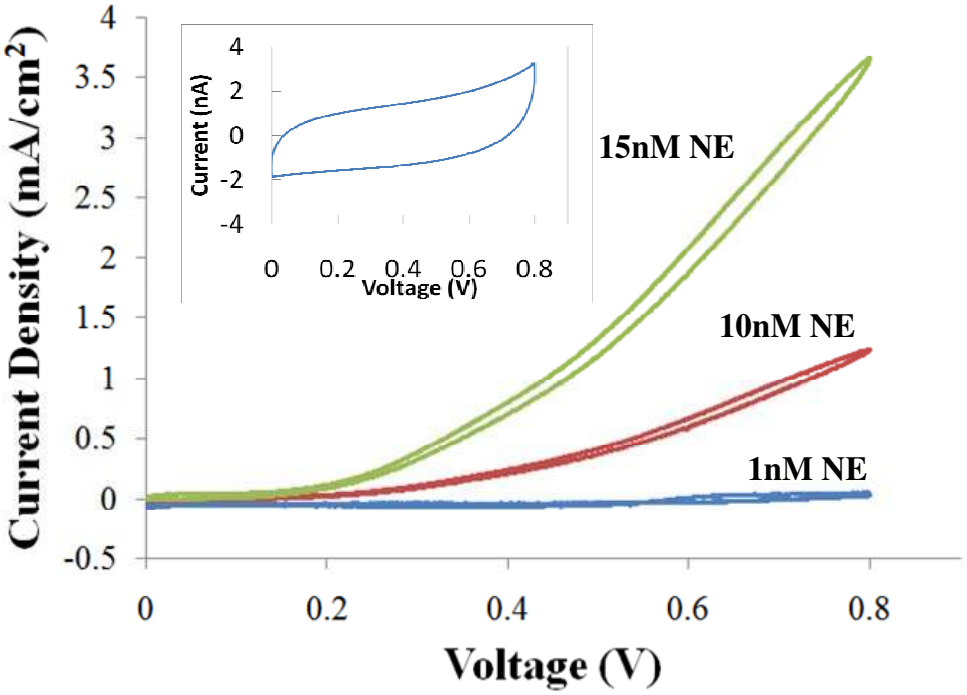

Fig. 11. Measured cyclic voltammogram of the poly-C probe for different concentrations of NE in Krebs buffer solution using scan rate of100 mV/s. The inset shows the background current in Krebs solution.

C. Acute in vivo Recording Using Diamond Probe

Microfabricated poly-C probes are used for the first time to record *in vivo* neural activity by surgically inserting the probe into the auditory cortex area of a guinea pig brain as shown in Fig. 12. The poly-C probe was mounted on a probe connector which is precisely controlled by a sub-micron positioner. During the electrical data recording, a broadband sound signal applied twice per second to stimulate the brain of the guinea pig. The poly-C probe monitored the effect of the sound signal on the neural activity inside the cortex; the result is shown in Fig. 13. The recorded electrical signal was amplified and filtered using a bandpass filter designed to pass frequencies in the 100 Hz - 10kHz range. It can be seen in Fig. 13(b) that the probe received a large signal of >25μV in response to the sound signal. It is demonstrated that the diamond probe received the stimulated neural signal at a signal to noise (S/N) ratio of ~2. There are several possible reasons for the low S/N ratio. One of the possible reasons is that the probe position may not be close enough to the body of the firing neurons. The strength of the neuron signal attenuates with increasing distance between the recording site and target neurons [53]. Increasing the SNR will be a priority in future work.

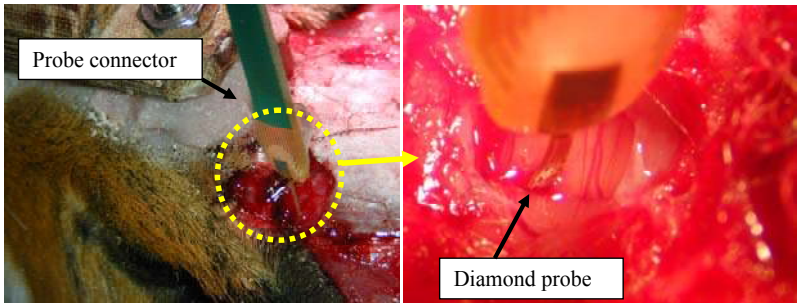

Fig. 12. Acute recording of neural activity using the diamond probe.

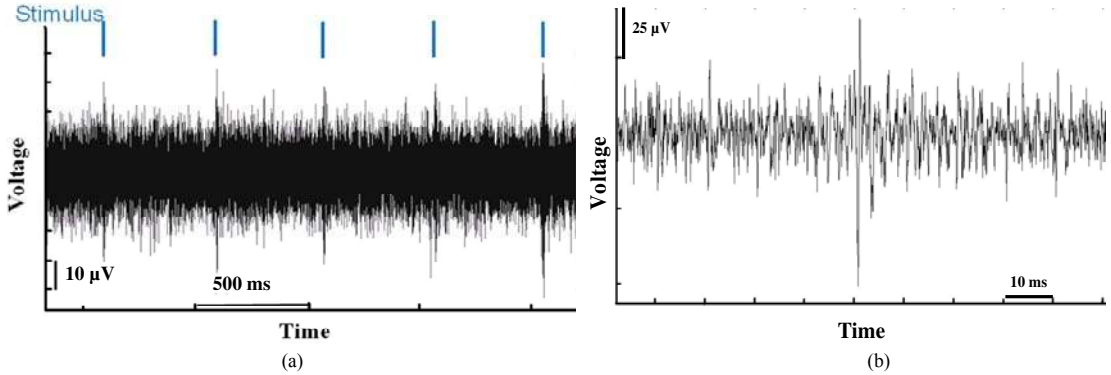

Fig. 13. (a) Recorded neural activity in guinea pig's auditory cortex using the diamond probe with an electrode area of 100μm^2, (b) A recorded neural spike.

5. CONCLUSIONS

For the first time, the design, fabrication and testing of a novel polycrystalline diamond (poly-C) based microprobe is reported for possible applications in neural prosthesis. The probe utilizes undoped poly-C with a resistivity in the range of 10^5 Ωcm as a mechanical material, which has a young's modulus in the range of 400 – 1,000 GPa and is biocompatible. Boron doped poly-C with a resistivity in the range of 10^{-3} Ωcm is used as an electrode material, which provides a chemically stable surface for both chemical and electrical detections in neural studies. The probe has eight poly-C electrode sites with diameters ranging from 2 to 150 μm; the electrode capacitance is approximately 87 μF/cm^2. The measured water potential window of the poly-C electrode spans across negative and positive electrode potentials and typical has a total value of 2.2 V in 1M KCl; the lowest detectable concentration of norepinephrine was on the order of 10 nM. The poly-C probe has also been successfully implanted in the auditory cortex area of guinea pig brain for *in vivo* neural studies. The recorded signal amplitude was 30-40 μV and had a duration of 1ms.

ACKNOWLEDGEMENT

This work is supported by the Engineering Research Centers Program (ERC) of the National Science Foundation under Award Number EEC-9986866. The authors are indebted to Ken Wise for his continue support and critical reading of the manuscript. The authors are thankful to Mike Varney and Sean Hatch for helpful discussion related to work reported in this paper.

REFERENCES

[1] K. D. Wise, J. B. Angell and A. Starr, "An integrated-circuit approach to extracellular microelectrodes," *IEEE Trans. Biomed. Eng.*, v.17, no. 3, pp. 238-247, 1970.

[2] P. Norlin, M. Kindlundh, A. Mouroux, K. Yoshida and U. G. Hofmann, "A 32-site neural recording probe fabricated by DRIE of SOI substrates," *J. of Micromech.& Microeng.*, pp. 414-419, 2002.

[3] D. R. Kipke, "Implantable neural probe systems for cortical neuroprosthesis," in *Proc. of Int. Conf. of the IEEE Eng. in Med. and Bio. Soc.*, pp. 5344-5347, 2004.

[4] Q. Bai and K. D. Wise, "Single-unit neural recording with active microelectrode arrays," *IEEE Trans. Biomed. Eng.*, v. 48, pp. 911-920, 2001.

[5] C. Pang, J. G. Cham, Z. Nenadic, S. Musallam, Y. C. Tai, J. W. Burdick and R. A. Andersen, " A new multi-site probe array with monolithically integrated parylene flexible cable for neural prostheses," in *Proc. of Int. Conf. of the IEEE Eng. in Med. and Bio. Soc*., pp. 7114- 7117, 2005.

[6] J. Chen and K. D. Wise, "A multichannel neural probe for selective chemical delivery at the cellular level," *IEEE Tans. Biomed Eng.*, v. 44, no. 8, pp. 760-769, 1997.

[7] L. Lin and A. Pisano, "Silicon processed microneedles," *IEEE J. Micromech. Syst.*, v. 8, no. 1, pp. 78-84, 1999.

[8] J. Wang, M. Gulari, P. T. Bhatti, B. Y. Arcand, K. Beach, C. R. Fredrich and K. D. Wise,, "A cochlear electrode array with built-in position sensing," in *Proc. of Int. Conf. on MEMS*, pp. 786-789, 2005.

[9] Y. Tang, D. M. Aslam, J. Wang and K. D. Wise, "Poly-Crystalline diamond piezoresistive position sensors for cochlear implant probe," in *Proc. of Solid-State Sensors, Actuators and Microsystems*, v.1, pp. 542-546, 2005.

[10] Y. Yao, M. N. Gulari, J. A. Wiler and K. D. Wise, "A microassembled low-profile three-dimensional microelectrode array for neural prosthesis applications", *J. of Micro. Mech. Syst.*, v. 16, no. 4, pp. 977-988, 2007.

[11] C. Pang, J. G. Cham, Z. Nenadic, Y. C. Tai, J. W. Burdick and R. A. Andersen, "A new neural recording electrode array with parylene insulating layer," in *Proc. of Int. Conf. on Miniaturized Syst. for Chemistry and Life Sciences*, pp. 675-677, 2005.

[12] E. Patrick, M. Ordonez, N. Alba, J. C. Sanchez and T. Nishida, "Design and fabrication of a flexible substrate microelectrode array for brain machine interfaces," in *Proc. of IEEE EMBS*, pp. 2966-2969, 2006.

[13] Y. Kato, M. Nishino, I. Saito, T. Suzuki and K. Mabuchi, "Flexible intracortical neural probe with biodegradable polymer for delivering bioactive components," in *Proc. of IEEE EMBS*, pp. 143-146, 2006.

[14] S. Takeuchi, T. Suzuki, K. Mabuchi and H. Fujita, "3D flexible multichannel neural probe array," *J. Micomech. Microeng.*, v. 14, pp. 104-107, 2004.

[15] H. Lu, S. H. Cho, J. B. Lee, L. Cauller, M. R. Ortega and G. Hughes, "SU8-based micro neural probe for enhanced chronic in-vivo recording of spike signals from regenerated axons," in *Proc. of IEEE Int. Conf. on Sensors*, pp. 66-69, 2006.

[16] M. D. Johnson, R. K. Franklin, K. A. Scott, R. B. Brown and D. R. Kipke, "Neural probes for concurrent detection of neurochemical and electrophysiological signals in vivo," in *Proc. of IEEE EMBS*, pp. 7325-7328, 2005.

[17] K. L. Drake, K. D. Wise, J. Farraye, D. J. Anderson and S. P. Bement, "Performance of planar multisite microprobes in recording extracelluar single-unit intracortical activity," *IEEE Trans. on biomedical eng.*, v. 35, no. 9, pp. 719-732, 1988.

[18] T. L. Rose, E. M. Kelliher and L. S. Robbless, "Assessment of capacitor electrodes: preliminary evaluation," *J. of Neurosci. Methods*, no. 12, pp. 181-193, 1985.

[19] D. J. Anderson, K. Najafi, S. J. Tanghe, D. A. Evans, K. L. Levy, J. F. Hetke, X. Xue, J. J. Zappia and K. D. Wise, "Batch-fabricated thin-film electrodes for stimulation of the central auditory system," *IEEE Trans. of Bio. Eng.*, v. 36, no. 7, 1989.

[20] M. P. Hughes, K. Bustamante, D. J. Banks and D. J. Ewims, "Effects of electrode size on the performance of neural recording microelectrodes," in *Proc. of IEEE Conf. on Microtech. in Med. And Bio.*, pp. 220-223, 2000.

[21] J. A. Stamford, P. Palij, C. Davidson, C. M. Jorm and J. Millar, "Simultaneous 'real time' electrochemical and electrophysiological recording in brain slices with a single carbon-fibre microelectrode," *J. of Neuroscience Methods*, v. 50, pp. 279-290, 1993.

[22] L. S. Pan, D. R. Kania, *Diamond: electronic properties and applications*, Springer, 1994.

[23] M. Hupert, A. Muck, J. Wang, J. Stotter, Z. Cvackova, S. Haymond, Y. Show and G. M. Swain, "Conductive diamond thin-films in

electrochemistry," *Dia. and Rel. Mat.*, v. 12, pp. 1940-1949, 2003.

[24] A.N. Ndao, F. Zenia, A. Deneuville, M. Bernard, C. L. le´ment, "Effect of boron concentration on the electrochemical reduction of nitrates on polycrystalline diamond electrodes, " *Dia. and Rel. Mat.*, v. 9, pp. 1175-1180, 2000.

[25] A. Bennett, J. Wang, Y. Show and G. M. Swain, "Effect of sp2-bonded nondiamond carbon impurity on the response of boron-doped polycrystalline diamond thin-film electrodes," *J. of Electrochem. Soc.*, v. 151, no. 9, pp. 306-313, 2004.

[26] C. E. Nebel, H. Kato, B. Rezek, D. Shin, D. Takeuchi, H. Watanabe and T. Yamamoto, "Electrochemical properties of undoped hydrogen terminated CVD diamond," *Dia. and Rel. Mat*., v. 15, pp. 264-268, 2006.

[27] G. M. Swain and R. Ramesham, "The electrochemical activity of boron-doped polycrystalline diamond thin film electrode," *Anal. Chem.*, v. 65, pp. 345-351, 1993.

[28] L. Tang, C. Tsai, W. W. Gerberich, L. Kruckeberg and D. R. Kania, "Biocompatibility of chemical-vapour-deposited diamond," *Biomaterials*, v. 16, pp. 483-488, 1995.

[29] R. A Freitas, Nanomedicine, *Vol. IIA: Biocompatibility*, Landes Bioscience, 2003.

[30] E. W. Salzman, J. Linden, G. McManama and J. A. Ware, "Role of fibrinogen in activation of platelets by artificial surfaces," *Annals N. Y. Acad. Sci*, v. 516, pp. 184-195, 1987.

[31] A. Kraft, "Doped diamond: A compact review on a new, versatile, electro material," *Int. J. Electrochem. Sci.*, v. 2, pp. 355-385, 2007.

[32] J. Cvacka, V. Quaiserova, J. W. Park, Y. Show, A. Muck and G. M. Swain, "Boron-doped diamond microelectrodes for use in capillary electrophoresis with electrochemical detection," *Anal. Chem*., v.75, pp. 2678-2687, 2005.

[33] J. M. Halpern, S. Xie, G. P. Sutton, B. T. Higashikubo, C. A. Chestek, H. Liu H. J. Chiel, and H. B. Martin, "Diamond electrodes for neurodynamic studies in Aplysia californica," *Dia. and Rel. Mat.*, v. 15, pp. 183-187, 2006.

[34] J. Park, V. Q. Mocko, K. Peckova, J. J. Galligan, G. D. Fink and G. M. Swain, " Fabrication, characterization, and application of a diamond microelectrode for electrochemical measurement of norepinephrine release from the sympathetic nervous system," *Dia. and Rel. Mat.*, v. 15, pp. 761-772, 2006.

[35] L. S. Pan and D. R. Kania, *Diamond: electronic properties and applications*, Springer, 1994.

[36] H. Liu and D. S. Dandy, "Studies on nucleation process in diamond CVD: an overview of recent developments," *Dia. and Rel. Mat.*, v. 4, no. 10, pp. 1173-1188, 1995.

[37] Y. Tang and D. M. Aslam, "Technology of polycrystalline diamond thin films for microsystems applications," *J. Vac. Sci. Technol.*, v. 3, pp. 1088-1095, 2005.

[38] K. Hermansson, U. Kindberg, B. Hok, G. Palmskoq, "Wetting properties of silicon surfaces," in *Proc. of IEEE Int. Conf. on Solid-State Sensors and Actuators*, pp. 193-196, 1991.

[39] Y. Ando, Y. Niishibayashi, K. Kobashi, T. Hirao and K. Oura, "Smooth and high-rate reactive ion etching of diamond," *Dia. and Rel. Mat.*, v. 11, pp. 824-827, 2002.

[40] I. Bell, M. K. Fung, W.J Zhang, K. H. Lai, Y. M. Wang, Z. F. Zhou, R. K. W. Yu, C. S. Lee and S. T. Lee, "Effects at reactive ion

etching of CVD diamond," *Thin Solid Films*, v. 368, pp. 222-226, 2000.

[41] G. F. Ding, H. P. Mao, Y. L. Cao, Y. H. Zhang, X. Yao and X. L. Zhao, "Micromachining of CVD diamond by RIE for MEMS applications," *Dia. and Rel. Mat*., v. 14, pp. 1543-1548, 2005.

[42] O. Dorsch, M. Werner and E. Obermeier, "Dry etching of undoped and boron doped polycrystalline diamond films," *Dia. and Rel. Mat.*, v. 4, pp. 456-459, 1995.

[43] Z. L. Cao, H. Y. Chan and D. M. Aslam, "Polycrystalline diamond technology in micropackaging," *in preparation*.

[44] H. –Y. Chan, D. M. Aslam, S. Wang, G. M. Swain and K. D. Wise, "Fabrication and testing of a novel all-diamond neural probe for chemical detection and electrical sensing applications," in *Proc. of Int. Conf. on MEMS*, pp. 244-247, 2008.

[45] J. E. B. Randles, "Kinetics of rapid electrode reactions. Part 3. – electron exchange reactions," *KW Somerton Trans. of the Faraday Society*, v. 48, pp. 937-950, 1952.

[46] A. J. Bard and L. R. Faulkner, *Electrochemical methods: fundamentals and applications*, Wiley Publishers, 2000.

[47] J. Xu, Q. Chen and G. M. Swain, "Anthraquinonedisulfonate electrochemistry: A comparison of glassy carbon, hydrogenated glassy carbon, highly oriented pyrolytic graphite, and diamond electrodes," *Anal. Chem.*, v. 70, pp. 3146-3154, 1998.

[48] R. Ramesham and M. F. Rose, "Cyclic voltammetric, a. c. and d. c. polarization behavior of boron-doped CVD diamond," *Thin Solids Films*, v. 300, pp. 144-153, 1997.

[49] A. Fujishma, Y. Einaga, T. N. Rao and D. A. Tryk, *Diamond electrochemistry*, Elsevier, 2005.

[50] J. D. Weiland, "Electrochemical properties of iridium oxide stimulating electrodes," Ph.D. dissertation, University of Michigan, 1997.

[51] L. S. Robbless, J. L. Lefko and S. B. Brummer, "Activated Ir: An electrode suitable for reversible charge injection in saline solution," *J. Electrochem. Soc*., v. 130, no. 3, pp. 731-732, 1983.

[52] J. Mozota and B. E. Cnway, "Surface and bulk process at oxidized iridium electrodes – I. Monolayer stage and transition to reversible multilayer oxide film behavior," *Electrochim. Acta*, v. 28, pp. 1-8, 1983.

[53] V. S. Polikov, P. A. Tresco, W. M. Reichert, "Response of brain tissue to chronically implanted neural electrodes," *J. of Neuroscience Method*, v. 148, pp. 1-18, 2005.